

Re-evaluating
FRIDGE

J. Schrod et al.

This discussion paper is/has been under review for the journal Atmospheric Measurement Techniques (AMT). Please refer to the corresponding final paper in AMT if available.

Re-evaluating the Frankfurt isothermal static diffusion chamber for ice nucleation

J. Schrod¹, A. Danielczok¹, D. Weber¹, M. Ebert², E. S. Thomson³, and H. G. Bingemer¹

¹Institute for Atmospheric and Environmental Sciences, J. W. Goethe-University, Frankfurt am Main, 60438 Frankfurt, Germany

²Institute for Applied Geosciences, Technical University of Darmstadt, 64287 Darmstadt, Germany

³Department of Chemistry and Molecular Biology, Atmospheric Science, University of Gothenburg, 41296, Gothenburg, Sweden

Received: 11 November 2015 – Accepted: 17 November 2015 – Published: 1 December 2015

Correspondence to: E. S. Thomson (erik.thomson@chem.gu.se)

Published by Copernicus Publications on behalf of the European Geosciences Union.

Title Page

Abstract

Introduction

Conclusions

References

Tables

Figures



Back

Close

Full Screen / Esc

Printer-friendly Version

Interactive Discussion



Abstract

Recently significant advances have been made in the collection, detection, and characterization of ice nucleating particles (INP). Ice nuclei are particles that facilitate the heterogeneous formation of ice within the atmospheric aerosol by lowering the free energy barrier to spontaneous nucleation and growth of ice from atmospheric water and/or vapor. The Frankfurt isostatic diffusion chamber (FRIDGE) is an INP collection and offline detection system that has become widely deployed and shows additional potential for ambient measurements. Since its initial development FRIDGE has gone through several iterations and improvements. Here we describe improvements that have been made in the collection and analysis techniques. We detail the uncertainties inherent in the measurement method, and suggest a systematic method of error analysis for FRIDGE measurements. Thus what is presented herein should serve as a foundation for the dissemination of all current and future measurements using FRIDGE instrumentation.

1 Introduction

Presently significant scientific resources are focused on identifying and categorizing what types of particles within the atmosphere are active ice nuclei. Ice nucleating particles (INP) are particles suspended within the atmosphere that lower the free energy barrier that exists to spontaneous nucleation. Thus INP are the low temperature analog to cloud condensation nuclei (CCN), which assist the nucleation of liquid droplets in the atmosphere. Almost any type of solid particle can help to nucleate ice in the atmosphere, but it remains an open question what types of particles are best able to lower the barrier to heterogeneous nucleation. Many aerosol particles such as mineral dust and primary biological particles have been identified as ice nucleators, yet the measured abundance of such INP does not jibe with observed macroscopic features of clouds, wherein a host of complicated and dynamic interactions lead to ice parti-

Re-evaluating FRIDGE

J. Schrod et al.

Title Page

Abstract

Introduction

Conclusions

References

Tables

Figures



Back

Close

Full Screen / Esc

Printer-friendly Version

Interactive Discussion



**Re-evaluating
FRIDGE**

J. Schrod et al.

Title Page

Abstract

Introduction

Conclusions

References

Tables

Figures



Back

Close

Full Screen / Esc

Printer-friendly Version

Interactive Discussion



cles (DeMott et al., 2011). Although some of the mechanisms of ice multiplication are known (Hallett and Mossop, 1974), it remains a significant scientific hurdle to identify the substances and processes that control the formation of cloud ice and precipitation.

The FRankfurt Ice nucleation Deposition freezinG Experiment (FRIDGE) is a system that pairs electrostatic precipitation of particles onto Si-wafers in a collection unit with an isostatic diffusion chamber for the activation, growth, and optical detection of ice on ice nucleating particles. The instrument and technique have been previously discussed (Bundke et al., 2008; Klein et al., 2010a) and since the original development, new multiple sampling (Sect. 2 and Schrod et al., 2013) and measurement chamber units (Jiang et al., 2015; Ardon-Dryer and Levin, 2014) have been built. As with any of the current measurement devices used to characterize ice nucleation, FRIDGE has strengths and weaknesses. Its principle strengths are the ease of aerosol collection and storage, which also allow for single particle electron microscopy analysis. In addition to the automated and remotely programmable collector described in Sect. 2, lightweight collection units have been manufactured that can be deployed onto unmanned aerial vehicles (Born et al., 2012; Lange et al., 2013). Sample wafers can be transported and stored easily for laboratory based analyses without any strict procedural precautions. A systematic study of wafers exposed to varying storage times and conditions shows little variation in resulting INP counts as described in Sect. 5.1. However, the analysis is time intensive and limited to deposition and condensation/immersion mode freezing behavior. Furthermore, after analysis the wafers collected in the sampling process must be prepared for reuse in a labor intensive multi-stage cleaning process. Thus the ratio of sampling time to processing time is one area of focus for continuous incremental improvement.

Since the FRIDGE instrument descriptions were first published by Bundke et al. (2008) and Klein et al. (2010a) there have been significant improvements in wafer analysis and the general understanding of results. Here we summarize recent experimental improvements made to FRIDGE, including a description of the automated PEAC7 sample collector, and report on errors that are contained in some of the previously

**Re-evaluating
FRIDGE**

J. Schrod et al.

Title Page

Abstract

Introduction

Conclusions

References

Tables

Figures



Back

Close

Full Screen / Esc

Printer-friendly Version

Interactive Discussion



published data from the FRIDGE method. The work includes a detailed analysis of these errors and proposes solutions for the FRIDGE user community. Furthermore, a detailed description of measurement uncertainties that must be considered when reporting FRIDGE measurement data is included. The methodological refinements come primarily in three broad areas; (i) improved experimental accuracy for determining nucleated ice, (ii) a clear and systematic understanding of particle and mass losses during the collection process, and (iii) a clear quantitative procedure for assessing the measurement uncertainty inherent in reported results.

The existing FRIDGE analysis chambers are all based on the Frankfurt design but have been used in various operating modes (Klein et al., 2010a; Jiang et al., 2015; Ardon-Dryer and Levin, 2014). In particular the Tel Aviv group have employed the FRIDGE chamber to study immersion mode freezing using droplet assays (Ardon-Dryer et al., 2011; Ardon-Dryer and Levin, 2014). Herein we focus on utilizing the FRIDGE technique with ice formation proceeding from a vapor saturated environment. Thus it should be clear that although the measurements we discuss at vapor pressures exceeding water saturation can encompass immersion mode freezing they do not involve freezing in macroscopic droplets. A useful discussion of the nuances pertaining to the pathways of freezing nucleation can be found in Vali et al. (2015) and the associated public discussion materials.

The simple design and operation of the FRIDGE collectors make the method uniquely suited to use as a monitoring tool. In this regard FRIDGE has been identified as an important resource in an effort to establish a global network of INP measurement data (Ansmann et al., 2014). Thus it is important that current and future results be understood in the context of the method's systematic error.

2 Automated and remotely controlled multiple sampling unit

A Programmable Electrostatic Aerosol Collector (PEAC7) has been developed for the automated sequential sampling of up to seven wafers. The PEAC7 is based on the

**Re-evaluating
FRIDGE**

J. Schrod et al.

Title Page

Abstract

Introduction

Conclusions

References

Tables

Figures



Back

Close

Full Screen / Esc

Printer-friendly Version

Interactive Discussion



design of the single wafer electrostatic aerosol collector as described in Klein et al. (2010a, b) but adds a rotatable wafer tray that includes seven sampling slots. In Fig. 1 a schematic and photograph of the unit are shown side-by-side. The main body of the sampler made from anodized aluminium consists of a cylindrical housing that encloses a concentric, rotatable plate. The plate rotation is powered by a stepper motor that can position each of seven machined wafer cavities in the sampling position below the charging unit. The charging unit and air intake are integrated into the top plate, which is secured to the underlying main body with a series of set screws during operation and can be removed to exchange the substrate wafers. When secured, an O-ring hermetically seals the top and bottom save for the inlet and outlet of the flow system. The aerosol being sampled is flowed through the unit at a set rate, while within the sampling chamber particles are negatively charged by collision with corona discharge electrons and are electrostatically precipitated onto the grounded Si-wafer underneath (the charging unit). The glass housing of the aerosol inlet and charging unit are clearly visible in Fig. 1. The stepper motor uses a neodymium magnet to calibrate the position of the disc, while a pump, a rotameter, a flow controller and a high voltage generator enable the sample collection and electrostatic precipitation. The entire unit is mounted in a standard 19 inch rack-mount case and uses a standard IEC 60320 C14 power inlet.

The PEAC7 can be programmed and directly controlled from a digital front panel or vis-à-vis serial communication with a computer through a RS-232 serial port. The unit is designed to allow for automated sampling using programmable date, time, wafer number (1–7), flow rate, and sampling duration. The computer link allows for remote control and thus monitoring and reprogramming of scheduled sampling tasks. A number of benefits arise from the use of automated PEAC7 sample collection, including the obvious advantages of reduced manual intervention. Most importantly the process of collecting regular measurements for long-term monitoring is highly simplified. This makes the PEAC7 uniquely suited to unstaffed and/or isolated stations that might be included in regional or global networks for INP monitoring.

3 Image analysis

The FRIDGE instrument relies on automated image analysis to identify and count nucleated ice particles on the collection substrates. Experiments demonstrate that the process of ice identification and INP counting are sensitive to illumination, camera resolution, and image contrast, and that the INP identification procedure used until 2012 introduced a systematic errors. Thus, FRIDGE data generated between 2008 and 2012 (data appears in the following publications, Bundke et al., 2008; Klein et al., 2010a, b; Bingemer et al., 2012; Niemand et al., 2012) have been identified to include erroneous measurements, resulting from the miscounting of liquid droplets as ice. Unfortunately, the full extent of the error is variable and depends upon the sampled aerosol, meaning that the entirety of data collected from the stated time period and reported in the cited publications must be invalidated. Likewise, any conclusions and proposed hypotheses based on INP counted by FRIDGE from those cited publications must be re-examined.

The experimental procedure and image processing using FRIDGE was previously summarized in Klein et al. (2010a). In this work we review details of the system where previous mistakes were made, and clarify how those mistakes have been (or should be) corrected.

When beginning a measurement water vapor is allowed to diffuse into the evacuated FRIDGE sample cell that encloses the wafer substrate on top of a cold stage, and ice grows on activated INP. The sample cells are analogous to environmentally controlled microscope stages with the substrate wafers replacing microscope slides. A CCD camera ($2/3''$ CCD ≥ 5 megapixels, 1 pixel $\approx 400 \mu\text{m}^2$) is used to monitor and record the sample substrates. LabView software is used to download images and detect changes in brightness on the aerosol collection wafer surface by comparing real time images with a reference image taken prior to the introduction of vapor. If more than $\mathcal{ST} \geq 30$ (previously $\mathcal{ST} \sim 4$) adjacent pixels, where \mathcal{ST} is used to indicate a size threshold, are bright enough to exceed a brightness threshold \mathcal{BT} , the area is counted as an ice crystal. Like \mathcal{ST} the currently utilized value for $\mathcal{BT} = 30$ exceeds the previously used

Re-evaluating FRIDGE

J. Schrod et al.

Title Page

Abstract

Introduction

Conclusions

References

Tables

Figures



Back

Close

Full Screen / Esc

Printer-friendly Version

Interactive Discussion



Re-evaluating
FRIDGE

J. Schrod et al.

Title Page

Abstract

Introduction

Conclusions

References

Tables

Figures



Back

Close

Full Screen / Esc

Printer-friendly Version

Interactive Discussion



parameters $\beta\mathcal{T} \sim 6$ by nearly an order of magnitude. Each pixel domain which exceeds these critical values is counted as an ice crystal and is assumed to originate from a single INP. The FRIDGE chamber has generally been operated in a water vapor regime that is super-saturated with respect to ice but sub-saturated with respect to liquid water.

This is done to prevent the miscounting of water droplets as ice crystals, although the current detection method also enables specific measurements above water saturation. Each wafer is monitored at set temperature and saturation conditions for 100 s, which is sufficient to activate all INP at the selected conditions.

The primary cause of image misinterpretation that existed in earlier FRIDGE measurements stemmed from water droplets being miscounted as ice crystals. This was somewhat a result of overly sensitive $S\mathcal{T}$ and $\beta\mathcal{T}$ parameters; but more significantly, studies targeting hygroscopic marine aerosol samples have made plain that such particles grow by condensation and deliquescence at lower than expected vapor saturations. Samples heavily loaded with marine aerosol showed unreasonably high levels of detected INP using the previous analysis technique, suggesting that hygroscopic aerosols were counted instead of INP. Furthermore, a re-analysis of archived data and image files demonstrates that many counted objects did not grow or change brightness over time as would be expected for ice crystals in an ice supersaturated environment. Rather, many particles tended to activate immediately upon access to water vapor and maintain a constant size throughout the experiments (Fig. 2). An amplification factor that was applied within the software to make small brightness changes visible to the observer further masked the error by limiting the range of distinguishable grey levels. In contrast to small hygroscopic particles, ice crystals appear as defined objects that grow rapidly and steadily in the ice supersaturated regime, and ultimately result in signals with size and brightness magnitudes larger than hygroscopic particles.

The effect is most easily recognized by examining particle growth originating from idealized aerosol particle samples. Figure 2 shows the mean diameter in pixels of counted objects using the outdated image processing algorithm for a hygroscopic salt sample (red line) and an efficient ice nucleating silver iodide sample (blue line). Shortly

**Re-evaluating
FRIDGE**

J. Schrod et al.

Title Page

Abstract

Introduction

Conclusions

References

Tables

Figures



Back

Close

Full Screen / Esc

Printer-friendly Version

Interactive Discussion



after the introduction of the water vapor the first signal appears in the salt sample, but as time elapses the mean size of the counted objects remains constant at 7 pixels. Contrastingly, the silver iodide sample shows a steady increase to a mean size of 600 pixels after 50 s. The phase of the objects counted by the algorithm can also be unraveled by analyzing the yield of detected objects in samples of hygroscopic and non-hygroscopic aerosols as a function of supersaturation with respect to ice and water (Fig. 3). This is done in Fig. 3, where the number of counted objects is plotted vs. relative humidity for both sea salt (a, b – hygroscopic) and silver iodide (c,d – non-hygroscopic, ice-nucleating) at three temperature conditions. The count number from the sea salt sample does not depend on ice supersaturation and even decreases slightly with colder temperatures. However, re-plotting the data vs. water saturation a correlation is observed, suggesting that there is a hygroscopic growth effect for liquid water. In contrast a strong exponential increase in count number as a function of ice supersaturation is visible in the silver iodide data.

Raw images of the wafers also show the clear difference between growing ice particles and small, stationary particles with microscopic amounts of surface bound water (Figs. 4 and 5). Repeated laboratory studies with well-known ice active aerosolized materials including silver iodide, Snomax®, and Arizona Test Dust consistently show the strong response of these particles as INP and their rapid growth, such as illustrated in Figs. 2, 3, and 4.

To verify that small, slow-growing ice crystals are not neglected in the counting scheme several experiments were performed with higher resolution optical methods. Both a light microscope and a high resolution lens (Navitar 12X Zoom) were utilized to observe in detail small subsections of wafer substrates in real-time as ice crystals and water droplets formed and metamorphosed (Fig. 5). Figure 5 shows a microscope image of a wafer with many small hygroscopic salt particles and a single ice active silver iodide particle sampled in separate sectors. The line demarcating the separation between microscopic droplets and a large ice crystal is clear. Light polarization was also used to distinguish liquid isotropic droplets from ice crystals. The anisotropy of ice

crystals ensures that reflected and refracted light intensity and polarization is a function of the incident parameters and geometry of the ice crystal (Thomson et al., 2009). Thus a polarization filter can be used to distinguish ice particles from unfrozen droplets (Fig. 6).

More high resolution imaging was used to examine the sub-pixel scale behavior of ice and droplet activation. Figure 7 shows the antiquated FRIDGE pixel domains (red grid) overlaying a high resolution image. The shaded stars illustrate the grey level change from the reference picture if such a difference exists, with the white stars indicating the changes which exceeded the $\beta\mathcal{T}$. The plot demonstrates two important aspects of the image processing. First, $\beta\mathcal{T}$ and $S\mathcal{T}$ must be chosen to allow objects to overlap pixel boundaries. In Fig. 7 the bright spherical object with a diameter of $18\ \mu\text{m}$ (growing from $6\ \mu\text{m}$ before the measurement) is smaller than even a single pixel, but yet it causes seven neighboring pixels to exceed $\beta\mathcal{T}$ and it therefore could be falsely counted as an ice crystal if $S\mathcal{T} \leq 7$ pixels. Secondly, it highlights the critical nature of the density of sampling. Clearly, too much particle loading on the sample will cause overlapping signals, but too few particles will make statistical analyses more difficult (cf., Sect. 5).

These findings have led to alterations of the image processing procedure. First, $\beta\mathcal{T}$ and $S\mathcal{T}$ are carefully chosen to maximize the signal to noise ratio. Second, objects which are observed not to grow in ice saturated conditions are not counted as ice. Establishing these restrictions for FRIDGE measurements means that as much as 99 % of previously counted objects are now neglected. As a consequence sampling volume, analysis temperatures and relative humidity conditions must be altered in order to obtain statistically meaningful INP counts on a substrate.

4 Particle losses

Previously, the FRIDGE electrostatic sampling unit collection efficiency has been reported as near 100 % over a wide range of sizes measured using a TSI 3936 Scanning Mobility Particle Sizer (SMPS; cf., Fig. 5 Klein et al., 2010a). More recently it

Re-evaluating FRIDGE

J. Schrod et al.

Title Page

Abstract

Introduction

Conclusions

References

Tables

Figures



Back

Close

Full Screen / Esc

Printer-friendly Version

Interactive Discussion



is has been suggested that 100 % retention efficiency, which was measured by Klein et al. (2010a) does not necessarily correspond to 100 % deposition onto the sampling wafers. With the PEAC7 a number of tests have been run to ascertain potential particle losses within the collector housing and to determine the fraction of particles deposited onto the wafers.

In order to assess the deposition efficiency of the electrostatic collector, tracer fluorescein natrium particles (Carl Roth Fluorescein-Natrium (C.I. 45350), Article Number 5283.1) were aerosolized by dry dispersion in compressed air and simultaneously measured in parallel using filter sampling (47 mm Fluoropore filters, 0.2 μm pore size, Merck Millipore Ltd.) and the PEAC7. In parallel with sampling, the size spectra of the generated aerosols were determined using a TSI 3330 optical particle sizer (OPS). After sampling the material is washed from the respective substrates by submerging in 25 mL deionized ultrasonic water baths. The washing water is analyzed for the concentration of dissolved fluorescein sodium using a HACH DR/2010 spectrophotometer. The fluorescein mass concentration can be related to the 494 nm absorption maximum using a calibration for concentration as a function of absorbance. From the measured absorbances a deposition efficiency \mathcal{E} can be calculated that corresponds to the ratio of material absorbed onto the wafer M_{waf} vs. the material absorbed by the filter M_{filt} ,

$$\mathcal{E} = \frac{M_{\text{waf}}}{M_{\text{filt}}}, \quad (1)$$

where the collection efficiency of the filter was verified to be unity using downstream sampling. Washing water was also used to irrigate the sample tubing to test for losses elsewhere in the collection system. Those tests were negative for fluorescein, and thus it is concluded that all particle losses occur within the FRIDGE wafer housing unit.

Figure 8 depicts measured deposition efficiencies for a range of fluorescein concentrations and varied particle size distributions expressed using the measured mean particle diameter. These systematic measurements show no correlation between either particle size or fluorescein concentration with deposition efficiency. By extension

Re-evaluating FRIDGE

J. Schrod et al.

Title Page

Abstract

Introduction

Conclusions

References

Tables

Figures

◀

▶

◀

▶

Back

Close

Full Screen / Esc

Printer-friendly Version

Interactive Discussion



Re-evaluating
FRIDGE

J. Schrod et al.

Title Page

Abstract

Introduction

Conclusions

References

Tables

Figures



Back

Close

Full Screen / Esc

Printer-friendly Version

Interactive Discussion



the combined measurements allow us to conclude that deposition efficiency will be similarly independent of number concentration. From the aggregate of experiments a mean collection efficiency $\bar{\mathcal{E}} \pm \Delta\mathcal{E} = 0.596 \pm 0.018$ is calculated, where $\Delta\mathcal{E}$ represents the standard error of the mean. Thus the particles deposited onto the FRIDGE wafers represent approximately 60 % of the total ambient particles.

A second test of the collection efficiency with aerosolized mineral hematite particles was undertaken by Scanning Electron Microscopy (SEM). The results from direct particle counting in the SEM were used as a verification test of the fluorescein results. Hematite was chosen as reference particles because its iron signature is easily identifiable using SEM and because the aerosolized hematite sample includes smaller particles (size distributions centered around 0.8–1.0 μm) that are not as abundant in the fluorescein samples. Using the SEM's high resolution imaging 33 cross sectional scans of three wafers with precipitated hematite were made. Each scan consisted of 33 images, each covering $3.7 \times 10^{-3} \text{ mm}^2$, thus resulting in total scanned areas of approximately 4 mm^2 per wafer. The scanned particle numbers were scaled by the areal ratio, assuming that the random SEM sampling procedure was representative of the total particle distribution. Thus the total particle number calculated from the SEM was compared with the particle number measured from the same aerosol using the TSI 3330 OPS to compute a mean efficiency of 60.3 %. The data presented in Table 1 illustrates that some uncertainty exists due to clustering of particles – lower and upper bounds correspond respectively to the assumptions that deposited agglomerates did or did not exist in the aerosol and thus were or were not present in the OPS counting. It is unknown if and how many clusters are present in the raw aerosol, however, some amount of clustering can be expected simply due to the deposition mechanism. Given the uncertainty and repetitive nature of individual particle counting the excellent agreement with the fluorescein is both edifying and remarkable.

Thus for the PEAC7 collector the identified mean collection efficiency $\bar{\mathcal{E}} \pm \Delta\mathcal{E} = 0.596 \pm 0.018$ and associated uncertainty must be considered when reporting measured INP concentrations as outlined in Sect. 5. Although deposition efficiencies are

not expected to vary significantly for other collectors, or collectors run under unusual collection conditions, investigators should be aware of potential variability.

5 Experimental repeatability and intrinsic uncertainties

Due to the time-consuming nature of routine FRIDGE analysis it is impossible to repeat individual wafer analysis to the extent that an ensemble of nucleation counts would be generated for every wafer. Thus there exists some intrinsic uncertainty to FRIDGE wafer analysis, in that repeated cooling cycles on a single wafer will yield some spread in the number of observed INP. Repetitive experiments have been conducted with exemplary wafers to illuminate the potential spread of INP results and a subset of examples are shown in Fig. 9. Repeating such measurements for many samples the weighted mean relative uncertainty in the counted absolute INP number is determined to be 18.3%. This reported uncertainty is taken from 20 wafers measured with between three and ten repetitions at eight temperature and saturation conditions (T , RH_i) = -15°C , 110%; -20°C , 120%; -25°C , 119%; -25°C , 126%; -30°C , 130%; -30°C , 132%; -32°C , 127%; -32°C , 134%) that cover the span of the conditions used in typical FRIDGE analyses.

Although in general statistical uncertainty is helped by increased sample size, in these analyses no trend in relative uncertainty is observed with total wafer count number. Therefore the reported relative error can be taken to be representative of the absolute count uncertainty for single measurements, and is valid over the range of parameter space accessible to FRIDGE analysis. However, there does exist an upper limit for the resolvable INP number that is defined by the ability to distinguish individual ice domains vis-à-vis the image analysis protocols (Sect. 3). Thus an upper bound of sampling density must be defined at the user level, but for typical conditions in the Frankfurt system average INP densities exceeding one INP per square millimeter become problematic.

Re-evaluating FRIDGE

J. Schrod et al.

Title Page

Abstract

Introduction

Conclusions

References

Tables

Figures



Back

Close

Full Screen / Esc

Printer-friendly Version

Interactive Discussion



Re-evaluating
FRIDGE

J. Schrod et al.

Title Page

Abstract

Introduction

Conclusions

References

Tables

Figures

◀

▶

◀

▶

Back

Close

Full Screen / Esc

Printer-friendly Version

Interactive Discussion



In addition to the uncertainty based upon the replicability of INP counts on a given wafer, some added uncertainty stems from the FRIDGE sampling units, which include flow regulators and as outlined for the PEAC7, programmable, timed sampling. Thus for each unit and sampling protocol the uncertainty of the flow (ΔF) and the timing (Δt) must be empirically determined. These uncertainties combined with the INP count uncertainty and the uncertainty in collection efficiency (Sect. 4) can be used to calculate the individual measurement uncertainty using standard error propagation techniques. For example the ambient INP concentration IN/L can be calculated from the number of INP counted on a single wafer,

$$\text{IN/L} = \frac{\text{IN}^{\#} - \text{IN}_{\text{blank}}^{\#}}{tF} \mathcal{E}^{-1}, \quad (2)$$

where the INP counted on a blank (clean) wafer under identical conditions $\text{IN}_{\text{blank}}^{\#}$ are subtracted from the INP counted on the sample wafer $\text{IN}^{\#}$ and divided by the total volume sampled as determined by the product of the sampling time t and the sampling flow rate F , modulo the collection efficiency \mathcal{E} . Thus the uncertainty in the concentration can be expressed as,

$$\Delta \text{IN/L} = |\text{IN/L}| \sqrt{\frac{(\Delta \text{IN}^{\#})^2 + (\Delta \text{IN}_{\text{blank}}^{\#})^2}{(\text{IN}^{\#} - \text{IN}_{\text{blank}}^{\#})^2} + \left(\frac{\Delta t}{t}\right)^2 + \left(\frac{\Delta F}{F}\right)^2 + \left(\frac{\Delta \mathcal{E}}{\mathcal{E}}\right)^2}, \quad \text{where} \quad (3)$$

$$\Delta \text{IN}^{\#} = 0.183(\text{IN}^{\#}) \quad \text{and} \quad \Delta \text{IN}_{\text{blank}}^{\#} = 0.183(\text{IN}_{\text{blank}}^{\#}). \quad (4)$$

In general the number of INP counted on blank wafers is small or zero and thus there is little or no contribution to the uncertainty from clean wafers. However, when analyzing wafers at low temperatures $T \leq -30^{\circ}\text{C}$ experimenters should cautiously verify the background detection from cleaned wafers. Similar error propagation procedures can be followed when calculating other quantities from INP counts measured using the FRIDGE system.

smallest activated fractions, or fewest INP, where the consequences of small changes in particle counts are amplified.

Repeated measurements at varying storage times make manifest the suitability of FRIDGE for monitoring applications and serve to reinforce the importance of clear and systematic approaches to the discussion of methodological uncertainties.

6 Re-evaluating FRIDGE using Saharan dust as a test case

On 16 April 2015 a Saharan dust event was sampled using the FRIDGE electrostatic deposition wafers at the Mt. Kleiner Feldberg, Taunus Observatory (826 m a.s.l., 50.221879° N, 8.446297° E). For completeness, a description of the dust event is included within the Supplement. Nine samples were taken over ≈ 6 h that day and were subsequently analyzed at -16 , -18 , -20 , -22 , and -24 °C at ice supersaturations straddling water saturation. In Fig. 11 the INP concentrations measured at $\text{RH}_{\text{water}} = 101\%$ are presented and compared with INP values calculated from the empirically-based immersion freezing parameterization model developed by DeMott et al. (2010) that has since been adapted specifically to mineral dust (DeMott et al., 2015). The latter were calculated using as input parameters, the aerosol size spectra concurrently measured at the site with a TSI 3330 OPS, and the nucleation temperature in Kelvin T_k . The DeMott et al. (2015) mineral dust parameterization,

$$n_{\text{INP}}(T_k) = (\text{cf})(n_{a>0.5\mu\text{m}})^{\alpha(273.16-T_k)+\beta} \exp(\gamma(273.16 - T_k) + \delta), \quad (5)$$

is based on Continuous Flow Diffusion Chamber (CFDC) measurements of both laboratory and naturally generated INP, and predicts INP concentration $n_{\text{INP}}(T_k)$ as a function of the total particle number concentration with diameters greater than $0.5 \mu\text{m}$ $n_{a>0.5\mu\text{m}} (\text{cm}^{-3})$ and the aforementioned temperature. The parameters cf , $\alpha = 0$, $\beta = 1.25$, $\gamma = 0.46$, $\delta = -11.6$, are empirically determined, with cf segregated to account for instrument-specific calibration factors. For laboratory data $\text{cf} = 1$, while for atmospheric data $\text{cf} = 3$ is shown to yield a better parametric fit. As shown in Fig. 11

Re-evaluating FRIDGE

J. Schrod et al.

Title Page

Abstract

Introduction

Conclusions

References

Tables

Figures



Back

Close

Full Screen / Esc

Printer-friendly Version

Interactive Discussion



Re-evaluating
FRIDGE

J. Schrod et al.

Title Page

Abstract

Introduction

Conclusions

References

Tables

Figures



Back

Close

Full Screen / Esc

Printer-friendly Version

Interactive Discussion



the FRIDGE data is best fit by the model using $cf = 0.636$, while maintaining $\alpha = 0$, $\beta = 1.25$, $\gamma = 0.46$, $\delta = -11.6$. It is impossible to determine whether the observed deviation from the earlier parametric fits results from instrumental differences or from the fact that the DeMott et al. (2015) parameterization was developed using experimental data measured at $RH_{\text{water}} = 105\%$. It is reasonable to assume that some combination of these effects yields the measured trend. However, given these differences the overall agreement with the DeMott et al. (2015) model is very strong over a broad range of temperature and more than three orders of magnitude of INP concentration.

The agreement of FRIDGE measurements with the DeMott et al. (2015) parameterization that is based on a host of data collected from both laboratory and field measurements for a variety of mineral dusts is not in itself proof that FRIDGE measurements yield strictly constrained absolute INP numbers. However, it is very convincing evidence that the uncertainties of the FRIDGE instrument are well enough constrained such that the measurements can be systematically compared with other reported INP data. Furthermore, DeMott et al. (2015) demonstrated their simple model to be in agreement with the more complex surface-area-based parameterization of Niemand et al. (2012). Niemand et al. (2012) utilized data from cloud chamber expansion experiments performed at the Aerosol Interaction and Dynamics in the Atmosphere (AIDA) facility to construct an immersion freezing parameterization, whereby temperature and dust particle surface area are used to calculate INP concentration. Thus the FRIDGE results are transitively linked with the experimental results from AIDA and therefore compare favorably with multiple natural and experimental systems.

7 Conclusions

The FRIDGE electrostatic deposition and wafer evaluation system for INP is a utilitarian tool for INP collection and evaluation that possesses several unique advantages. Collection units themselves are compact and simple to operate, and analysis for INP counting and particle characterization vis-à-vis Scanning Electron Microscopy can be done

**Re-evaluating
FRIDGE**

J. Schrod et al.

Title Page

Abstract

Introduction

Conclusions

References

Tables

Figures



Back

Close

Full Screen / Esc

Printer-friendly Version

Interactive Discussion



in controlled laboratory settings. For these reasons a network of FRIDGE sampling and analysis instruments has begun to emerge, targeting globally distributed long-term measurements. The PEAC7 we have described here is a remotely controlled collector that can be automated for intermittent sampling and has been designed to target monitoring applications.

Challenges for the FRIDGE system include technical limitations with regards to the method's temporal resolution and a previously flawed analysis system. The former challenge can and will be incrementally addressed to improve the sampling technique and chain of analysis. While those incremental changes will potentially improve spatial and temporal resolution they will not affect the underlying measurement principle and/or uncertainties.

Herein we have addressed the latter challenge by laying bare where problems have occurred in the past and how those problems can be systematically addressed to obtain accurate INP number results. First and foremost it is clear that a majority of counting error can result from the choice of image analysis parameters. Although the suggested values for image thresholds are not failsafe they should be taken as a guide and any FRIDGE user should be aware of the potential pitfalls detailed in Sect. 3. The FRIDGE collection system has also been re-examined and it has been determined that deposition to non-wafer parts of the collector housing account for particle losses within the system. Experiments utilizing fluorescein tagged aerosol particles determined a mean deposition collection efficiency of $\mathcal{E} \pm \Delta\mathcal{E} = 0.596 \pm 0.003$, a value which is supported by direct SEM counting of hematite particles. Similarly, repeated analysis of single wafers has helped to constrain the uncertainty of any single INP number measurement to be $\pm 18.3\%$. These factors plus any additional uncertainty in measurement duration and volume must be considered in order to construct a complete treatment of FRIDGE measurement uncertainty. Under most experimental conditions the repeatability will dominate other uncertainties, and thus $\pm 20\%$ is a useful guidepost for the intrinsic measurement uncertainty. However, as illustrated in Figs. 10 and 11 the natural variability typically observed outweighs the intrinsic uncertainty. Thus it is suggested that

**Re-evaluating
FRIDGE**

J. Schrod et al.

Title Page

Abstract

Introduction

Conclusions

References

Tables

Figures



Back

Close

Full Screen / Esc

Printer-friendly Version

Interactive Discussion



any communicated FRIDGE data should independently specify both this intrinsic measurement uncertainty and any statistical uncertainty associated with measurements whereby multiple sampling is used to illuminate variability.

A test case of the re-evaluated FRIDGE system illustrates agreement with other INP measurement methods that utilize both laboratory and natural aerosols. We find agreement up to -16°C with the parameterization previously developed by DeMott et al. (2015) that uses aerosol number concentration to predict INP concentration. Thus the FRIDGE observations further support the DeMott et al. (2015) hypothesis that laboratory results for ice nucleation in idealized systems have applicability to natural atmospheric aerosols. Although such parameterizations have begun to be used in prognostic ice nucleation schemes for cloud and climate models (Fan et al., 2014a, b), the FRIDGE work also makes clear that investigations must continue to strive for a deeper understanding of instrument dependent parametric variation, etc.

Significant resources and energy are currently focused on addressing the broad issues that surround inter-comparison of data collected using different techniques. In this regard FRIDGE has taken part in a series of instrument inter-comparisons, beginning in March 2015 with the Fifth International Ice Nucleation Workshop (FIN02) at the AIDA facility in Karlsruhe, Germany. There more than a dozen different ice nuclei counting instruments and techniques were collected to measure and compare various ice active materials in a rigorously designed laboratory environment. As a follow up FRIDGE joined the third component of the inter-comparison (FIN03) in September 2015, where measurements focused on utilizing multiple INP sampling techniques at a single field site (Storm Peak Laboratory, Steamboat Springs, CO, USA). Data analysis and synthesis from these campaigns is ongoing and will be available in upcoming publications. These efforts are expected to be a big step forward for the scientific understanding of how best to measure, characterize and systematically compare ice nuclei.

**The Supplement related to this article is available online at
doi:10.5194/amtd-8-12525-2015-supplement.**

Acknowledgements. Support and funding for this work was contributed by the Deutsche Forschungsgemeinschaft (DFG) under the Research Unit FOR 1525 (INUIT), the EU FP7-ENV-2013 BACCHUS project under Grant Agreement 603445, the Swedish Research Council, the Swedish Research Council FORMAS, and the Nordic Top-Level Research Initiative CRAICC.

5 References

Ansmann, A., Atkinson, J., Decesari, S., Bühl, J., Facchini, M. C., Gysel, M., Baltensperger, U., Herrmann, E., Connolly, P., Crooks, M., Rosenfeld, D., and Sierau, B.: Definition of the BACCHUS aerosol/cloud database (structure, contents), first preliminary data set (some cloud products from satellite observations and first CCN/IN data), Deliverable report, TROPOS, Leipzig, Germany, 2014. 12528

10 Ardon-Dryer, K. and Levin, Z.: Ground-based measurements of immersion freezing in the eastern Mediterranean, *Atmos. Chem. Phys.*, 14, 5217–5231, doi:10.5194/acp-14-5217-2014, 2014. 12527, 12528

15 Ardon-Dryer, K., Levin, Z., and Lawson, R. P.: Characteristics of immersion freezing nuclei at the South Pole station in Antarctica, *Atmos. Chem. Phys.*, 11, 4015–4024, doi:10.5194/acp-11-4015-2011, 2011. 12528

Bingemer, H., Klein, H., Ebert, M., Haunold, W., Bundke, U., Herrmann, T., Kandler, K., Müller-Ebert, D., Weinbruch, S., Judt, A., Wéber, A., Nillius, B., Ardon-Dryer, K., Levin, Z., and Curtius, J.: Atmospheric ice nuclei in the Eyjafjallajökull volcanic ash plume, *Atmos. Chem. Phys.*, 12, 857–867, doi:10.5194/acp-12-857-2012, 2012. 12530

20 Born, J., Möhler, O., Haunold, W., Schrod, J., Brooks, I., Norris, S., Brooks, B., Hill, M., and Leisner, T.: Meteorological and Aerosol Sensing with small Unmanned Aerial Systems, in: EGU General Assembly Conference Abstracts, edited by: Abbasi, A. and Giesen, N., vol. 14 of EGU General Assembly Conference Abstracts, Vienna, AT, 22–27 April 2012, p. 897, 2012. 12527

25 Bundke, U., Nillius, B., Jaenicke, R., Wetter, T., Klein, H., and Bingemer, H.: The fast Ice Nucleus chamber FINCH, *Atmos. Res.*, 90, 180–186, doi:10.1016/j.atmosres.2008.02.008, 2008. 12527, 12530

30 DeMott, P. J., Prenni, A. J., Liu, X., Kreidenweis, S. M., Petters, M. D., Twohy, C. H., Richardson, M. S., Eidhammer, T., and Rogers, D. C.: Predicting global atmospheric ice nuclei

Re-evaluating FRIDGE

J. Schrod et al.

Title Page

Abstract

Introduction

Conclusions

References

Tables

Figures



Back

Close

Full Screen / Esc

Printer-friendly Version

Interactive Discussion



Re-evaluating
FRIDGE

J. Schrod et al.

Title Page

Abstract

Introduction

Conclusions

References

Tables

Figures



Back

Close

Full Screen / Esc

Printer-friendly Version

Interactive Discussion



distributions and their impacts on climate, *P. Natl. Acad. Sci. USA*, 107, 11217–11222, doi:10.1073/pnas.0910818107, 2010. 12539

DeMott, P. J., Möhler, O., Stetzer, O., Vali, G., Levin, Z., Petters, M. D., Murakami, M., Leisner, T., Bundke, U., Klein, H., Kanji, Z. A., Cotton, R., Jones, H., Benz, S., Brinkmann, M., Rzesanke, D., Saathoff, H., Nicolet, M., Saito, A., Nillius, B., Bingemer, H., Abbatt, J., Ardson, K., Ganor, E., Georgakopoulos, D. G., and Saunders, C.: Resurgence in ice nuclei measurement research, *B. Am. Meteorol. Soc.*, 92, 1623–1635, doi:10.1175/2011BAMS3119.1, 2011. 12527

DeMott, P. J., Prenni, A. J., McMeeking, G. R., Sullivan, R. C., Petters, M. D., Tobo, Y., Niemand, M., Möhler, O., Snider, J. R., Wang, Z., and Kreidenweis, S. M.: Integrating laboratory and field data to quantify the immersion freezing ice nucleation activity of mineral dust particles, *Atmos. Chem. Phys.*, 15, 393–409, doi:10.5194/acp-15-393-2015, 2015. 12539, 12540, 12542, 12557

Fan, J., Leung, L. R., DeMott, P. J., Comstock, J. M., Singh, B., Rosenfeld, D., Tomlinson, J. M., White, A., Prather, K. A., Minnis, P., Ayers, J. K., and Min, Q.: Aerosol impacts on California winter clouds and precipitation during CalWater 2011: local pollution versus long-range transported dust, *Atmos. Chem. Phys.*, 14, 81–101, doi:10.5194/acp-14-81-2014, 2014a. 12542

Fan, J., Leung, L. R., DeMott, P. J., Comstock, J. M., Singh, B., Rosenfeld, D., Tomlinson, J. M., White, A., Prather, K. A., Minnis, P., Ayers, J. K., and Min, Q.: Corrigendum to Aerosol impacts on California winter clouds and precipitation during CalWater 2011: local pollution versus long-range transported dust published in *Atmos. Chem. Phys.*, 14, 81–101, 2014, *Atmos. Chem. Phys.*, 14, 3063–3064, doi:10.5194/acp-14-3063-2014, 2014b. 12542

Hallett, J. and Mossop, S. C.: Production of secondary ice particles during the riming process, *Nature*, 249, 26–28, doi:10.1038/249026a0, 1974. 12527

Jiang, H., Yin, Y., Su, H., Shan, Y., and Gao, R.: The characteristics of atmospheric ice nuclei measured at the top of Huangshan (the Yellow Mountains) in Southeast China using a newly built static vacuum water vapor diffusion chamber, *Atmos. Res.*, 153, 200–208, doi:10.1016/j.atmosres.2014.08.015, 2015. 12527, 12528

Klein, H., Haunold, W., Bundke, U., Nillius, B., Wetter, T., Schallenberg, S., and Bingemer, H.: A new method for sampling of atmospheric ice nuclei with subsequent analysis in a static diffusion chamber, *Atmos. Res.*, 96, 218–224, doi:10.1016/j.atmosres.2009.08.002, 2010a. 12527, 12528, 12529, 12530, 12533, 12534

Re-evaluating
FRIDGE

J. Schrod et al.

Title Page

Abstract

Introduction

Conclusions

References

Tables

Figures



Back

Close

Full Screen / Esc

Printer-friendly Version

Interactive Discussion



- Klein, H., Nickovic, S., Haunold, W., Bundke, U., Nillius, B., Ebert, M., Weinbruch, S., Schuetz, L., Levin, Z., Barrie, L. A., and Bingemer, H.: Saharan dust and ice nuclei over Central Europe, *Atmos. Chem. Phys.*, 10, 10211–10221, doi:10.5194/acp-10-10211-2010, 2010b. 12529, 12530
- 5 Lange, M., Argyrides, M., Ioannou, S., Keleshis, C., and Levin, Z.: Unmanned Aerial Systems as Versatile Tools for Atmospheric and Environmental Research, in: EGU General Assembly Conference Abstracts, vol. 15 of EGU General Assembly Conference Abstracts, Vienna, AT, 7–12 April 2013, p. 7851, 2013. 12527
- 10 Niemand, M., Möhler, O., Vogel, B., Vogel, H., Hoose, C., Connolly, P., Klein, H., Bingemer, H., DeMott, P., Skrotzki, J., and Leisner, T.: A particle-surface-area-based parameterization of immersion freezing on desert dust particles, *J. Atmos. Sci.*, 69, 3077–3092, doi:10.1175/JAS-D-11-0249.1, 2012. 12530, 12540
- Schrod, J., Bingemer, H., Haunold, W., Curtius, J., Decesari, S., Marinoni, A., Rinaldi, M., Bonasoni, P., and Cristofanelli, P.: Ice nuclei measurements at a high altitude remote station in the Northern Apennines, in: EGU General Assembly Conference Abstracts, vol. 15 of EGU General Assembly Conference Abstracts, Vienna, AT, 7–12 April 2013, p. 1925, 2013. 12527
- 15 Thomson, E. S., Wilen, L. A., and Wettlaufer, J. S.: Light scattering from an isotropic layer between uniaxial crystals, *J. Phys.-Condens. Mat.*, 21, 195407, doi:10.1088/0953-8984/21/19/195407, 2009. 12533
- 20 Vali, G., DeMott, P. J., Möhler, O., and Whale, T. F.: Technical Note: A proposal for ice nucleation terminology, *Atmos. Chem. Phys.*, 15, 10263–10270, doi:10.5194/acp-15-10263-2015, 2015. 12528

Re-evaluating
FRIDGE

J. Schrod et al.

Title Page

Abstract

Introduction

Conclusions

References

Tables

Figures

I◀

▶I

◀

▶

Back

Close

Full Screen / Esc

Printer-friendly Version

Interactive Discussion

**Table 1.** Particle data for SEM measurements.

| Wafer | OPS Total Particles | SEM Counted Particles | | SEM Total Particles | | Efficiency [%] | |
|-----------------------|---------------------|-----------------------|-------|---------------------|---------|----------------|-------|
| | | Bounds: Lower | Upper | Lower | Upper | Lower | Upper |
| 1* | 177 132 | 162 | 386 | 63 302 | 150 832 | 35.7 | 85.2 |
| 2 | 214 292 | 332 | 403 | 129 731 | 157 475 | 60.5 | 73.5 |
| 3 | 211 232 | 279 | 298 | 109 021 | 116 445 | 51.6 | 55.1 |
| Mean Efficiencies [%] | | | | | | 49.3 | 71.3 |
| | | | | | | 60.3 | |

* The heavy clustering observed in wafer 1 was subsequently minimized by using a cyclone separator to remove the large particle fraction.

Re-evaluating
FRIDGE

J. Schrod et al.

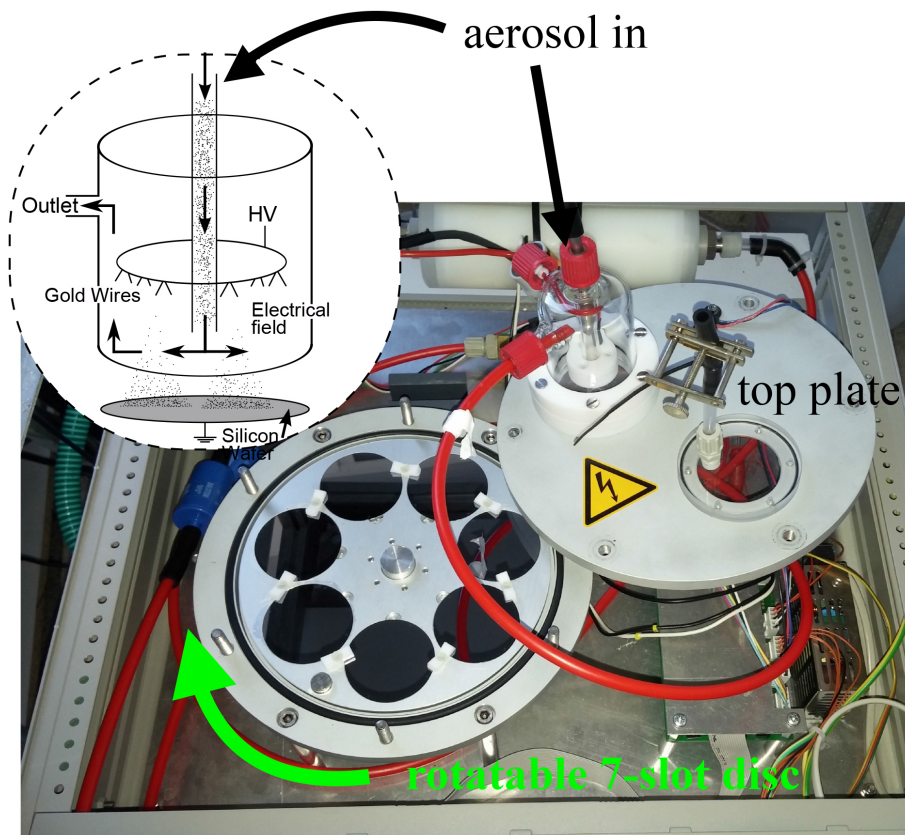


Figure 1. Picture of the PEAC7 multiple sampling unit with a schematic of the charging unit inset. For the photograph the top-plate containing the charging unit has been removed and offset to reveal the underlying rotatable disc with seven sample wafers mounted into machined slots.

Re-evaluating
FRIDGE

J. Schrod et al.

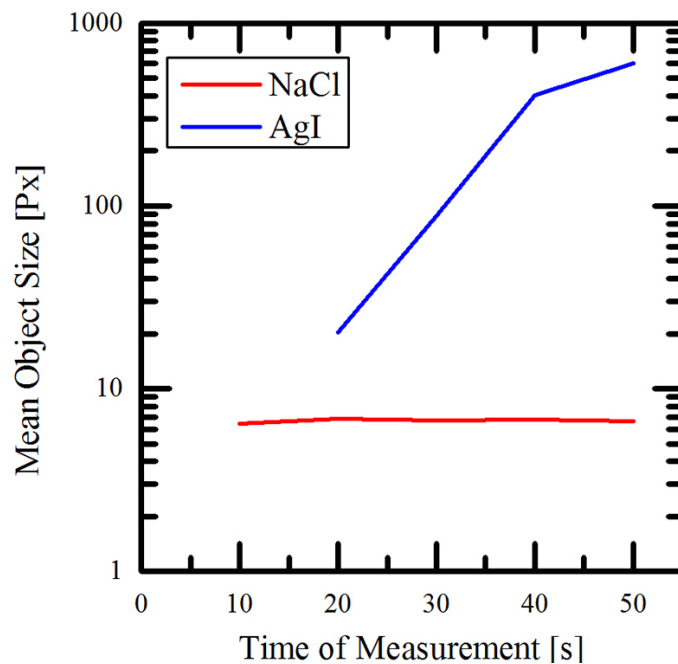


Figure 2. Mean object size in pixels for a strongly ice nucleating silver iodide sample (blue) and a hygroscopic NaCl salt sample (red) vs. the measurement time. Measurements made at -18°C and $\text{RH}_i = 118\%$.

[Title Page](#)[Abstract](#)[Introduction](#)[Conclusions](#)[References](#)[Tables](#)[Figures](#)[◀](#)[▶](#)[◀](#)[▶](#)[Back](#)[Close](#)[Full Screen / Esc](#)[Printer-friendly Version](#)[Interactive Discussion](#)

Re-evaluating
FRIDGE

J. Schrod et al.

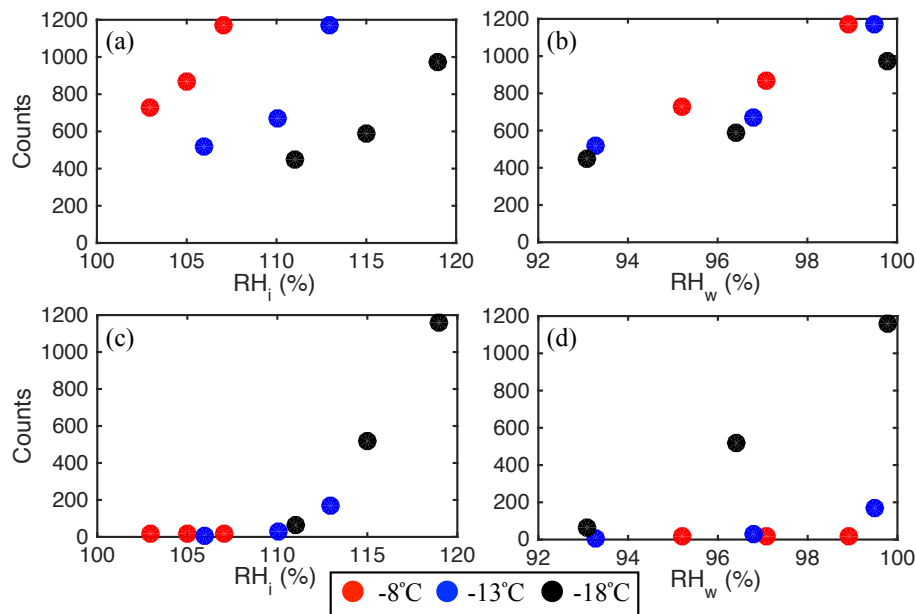


Figure 3. Number of counted INP on wafers with deposited sea salt (**a, b**) and silver iodide (**c, d**) particles vs. relative humidity with respect to ice (left panels) and water (right panels) for -8°C (red), -13°C (blue) and -18°C (black).

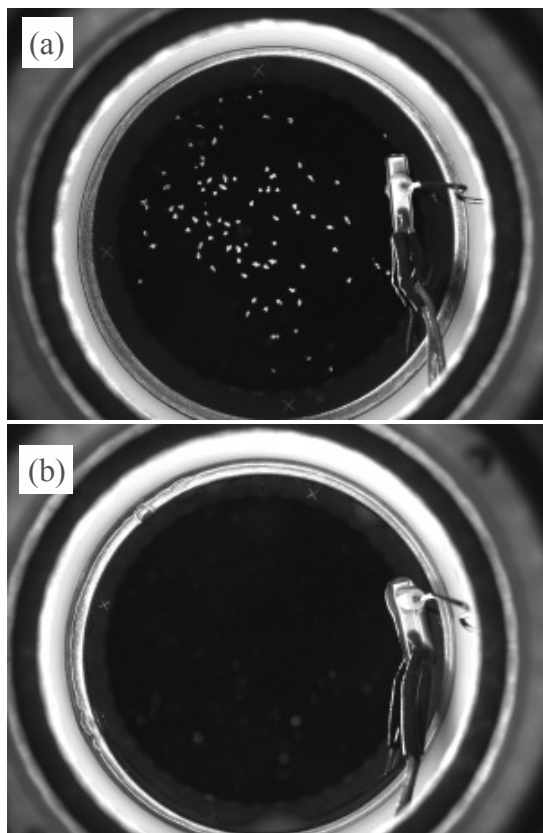


Figure 4. Unprocessed images of sample wafers 50 s after water vapour injection at $T = -18^{\circ}\text{C}$, $\text{RH}_i = 118\%$ for **(a)** silver iodide and **(b)** NaCl.

Title Page

Abstract

Introduction

Conclusions

References

Tables

Figures

◀

▶

◀

▶

Back

Close

Full Screen / Esc

Printer-friendly Version

Interactive Discussion



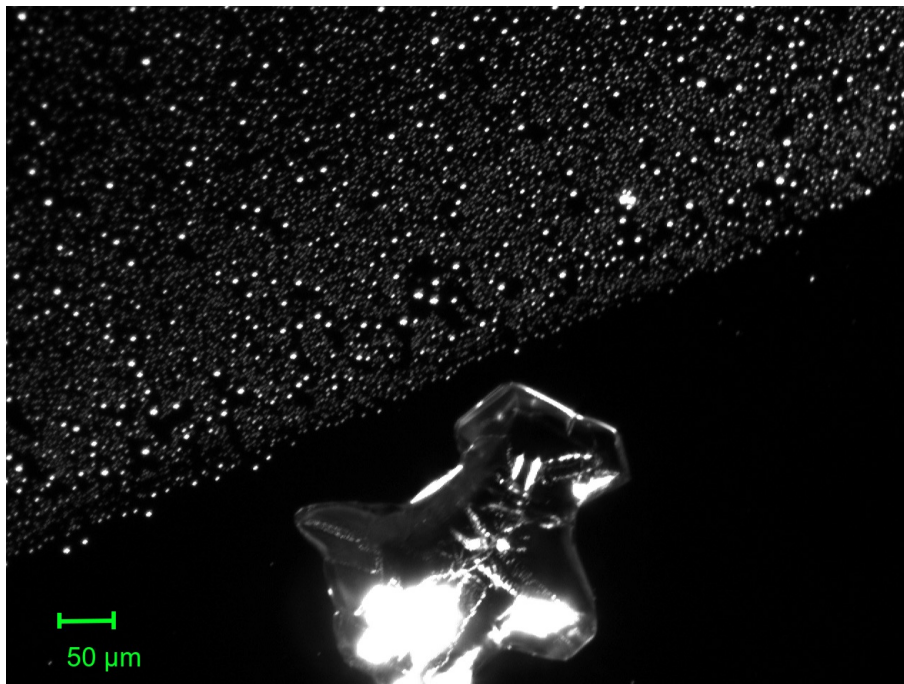


Figure 5. Microscope image of a sample laden with many small salt particles (upper left) and a single silver iodide particle (lower right). The hygroscopic salt facilitates the formation of many small spherical objects, while a distinct ice crystal grows on the sector with the deposited silver iodide.

Re-evaluating FRIDGE

J. Schrod et al.

Title Page

Abstract

Introduction

Conclusions

References

Tables

Figures

◀

▶

◀

▶

Back

Close

Full Screen / Esc

Printer-friendly Version

Interactive Discussion



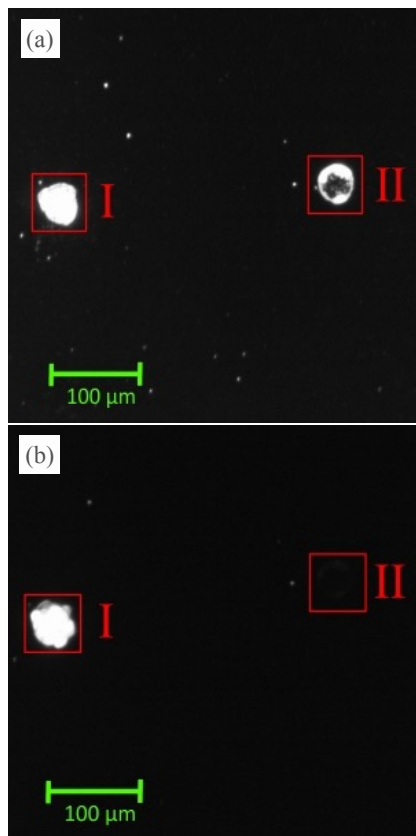


Figure 6. Successive microscopic images of a sample substrate **(a)** without using a polarization filter and **(b)** with the filter inserted. The latter highlights the use of polarized light to identify frozen ice (I) vs. a liquid droplet (II), whereby the birefringence of the ice crystal sufficiently alters the light polarization to allow it to pass through the filter.

Re-evaluating
FRIDGE

J. Schrod et al.

Title Page

Abstract

Introduction

Conclusions

References

Tables

Figures

◀

▶

◀

▶

Back

Close

Full Screen / Esc

Printer-friendly Version

Interactive Discussion

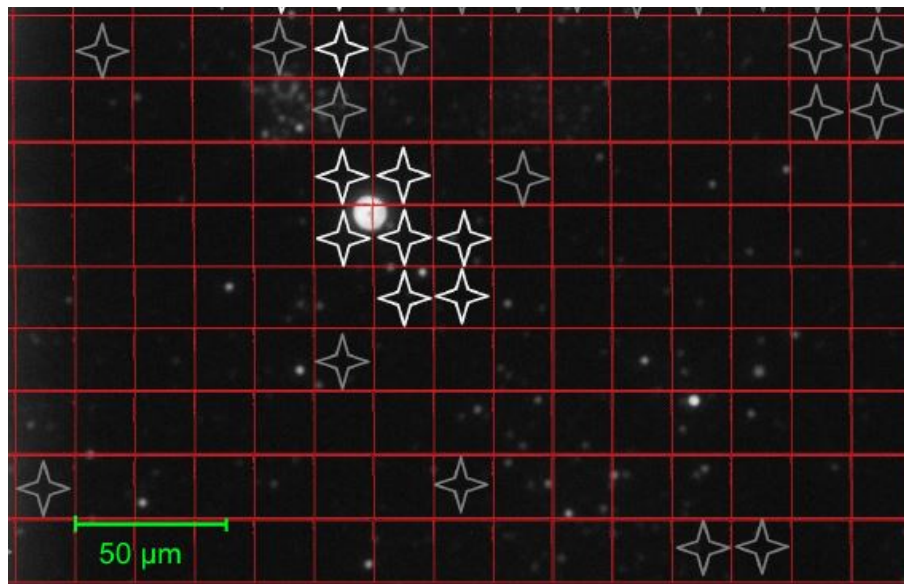


Figure 7. Overlay of high resolution substrate image taken using a Navitar 12× zoom lens and the outdated FRIDGE image processing (red grid cells = 1 Px, stars signal with which color those pixels would have been displayed).

Re-evaluating
FRIDGE

J. Schrod et al.

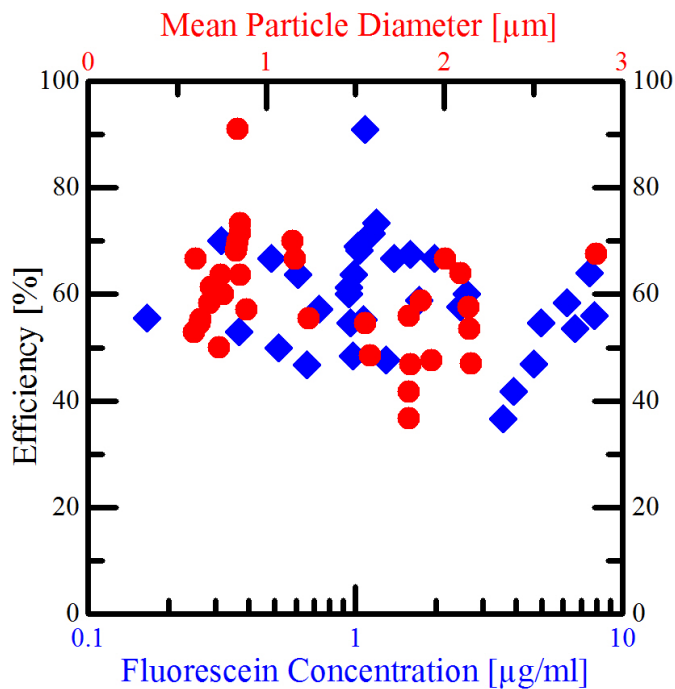


Figure 8. Measured deposition efficiency in a PEAC7 aerosol sampler for 35 samples, exhibiting a range of fluorescein concentrations (lower abscissa scale, blue diamonds) and mean particle diameters (upper abscissa scale, red dots).

[Title Page](#)[Abstract](#)[Introduction](#)[Conclusions](#)[References](#)[Tables](#)[Figures](#)[◀](#)[▶](#)[◀](#)[▶](#)[Back](#)[Close](#)[Full Screen / Esc](#)[Printer-friendly Version](#)[Interactive Discussion](#)

Re-evaluating
FRIDGE

J. Schrod et al.

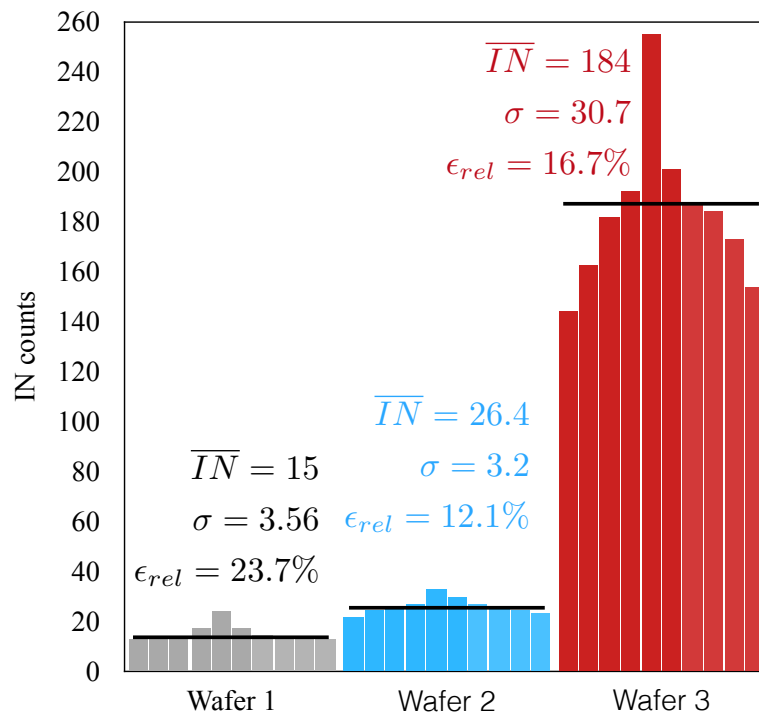


Figure 9. Example data from wafer measurements repeated ten times and reordered to resemble normal distributions. The weighted mean relative error determined from repeated measurements of 20 wafers (3–10 repetitions per wafer) is 18.3%.

Title Page

Abstract

Introduction

Conclusions

References

Tables

Figures

◀

▶

◀

▶

Back

Close

Full Screen / Esc

Printer-friendly Version

Interactive Discussion



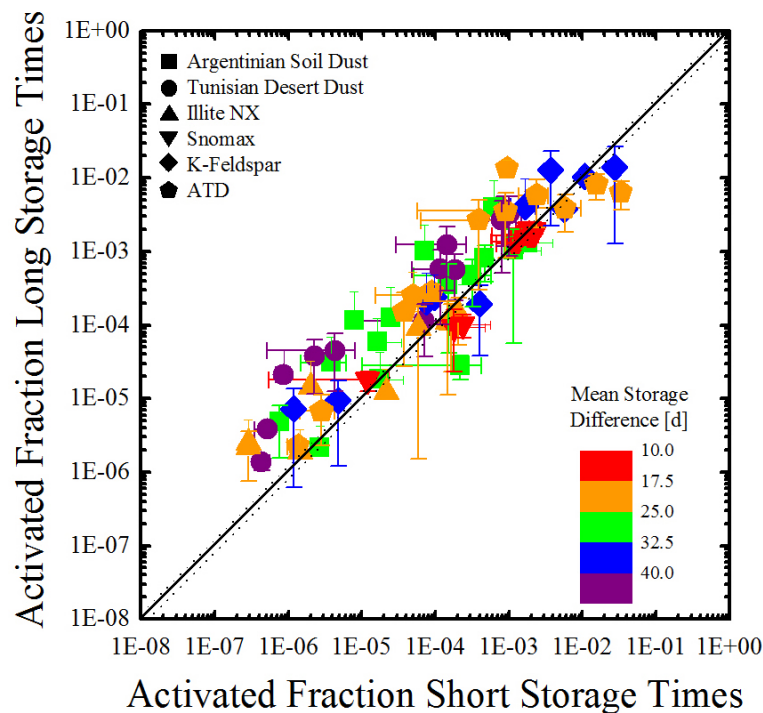


Figure 10. Effect of storage on sample integrity. Scatter plot of the fraction of INP activated in aerosol samples that were analyzed shortly after sampling (abscissa) vs. the same parameter for samples from the same aerosol that were analyzed after storage (ordinate). Symbols correspond to different test aerosols as indicated, while the color codes represent the average storage time difference between analyses.

Re-evaluating
FRIDGE

J. Schrod et al.

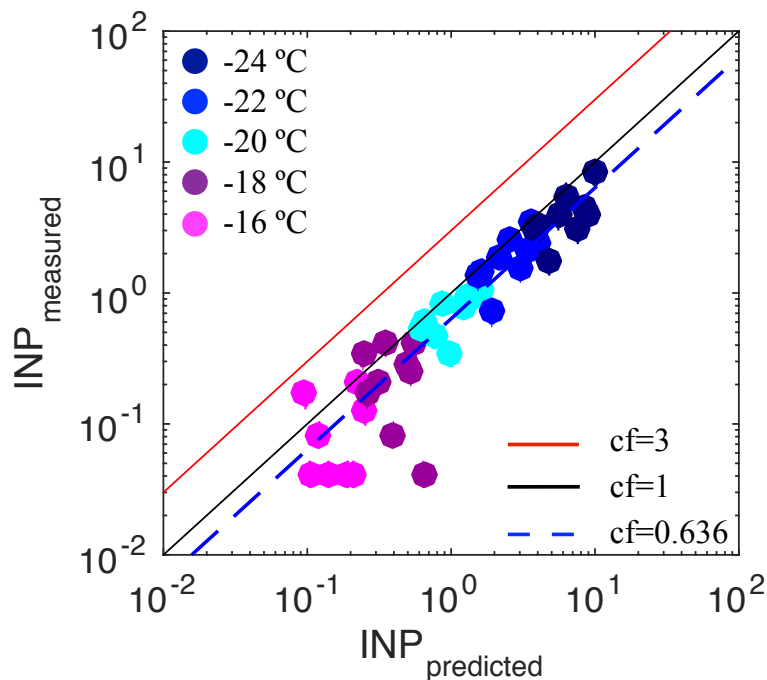


Figure 11. Measured INP concentrations vs calculated INP concentrations for mineral dust loaded aerosol transported to Mt. Kleiner Feldberg in April 2015. Error bars indicate the complete measurement uncertainty as enumerated in Eq. (3). The three lines correspond to three realizations of the DeMott et al. (2015) parameterization given three different calibration factors (Eq. 5). Where they do not appear error bars are subsumed by the points.

Title Page

Abstract

Introduction

Conclusions

References

Tables

Figures

◀

▶

◀

▶

Back

Close

Full Screen / Esc

Printer-friendly Version

Interactive Discussion

